

1 **Statistical Properties of Electron Curtain Precipitation**
2 **Estimated with AeroCube-6**

3 **M. Shumko^{1,2}, A.T. Johnson¹, T.P. O'Brien³, D.L. Turner⁴, A.D. Greeley²,**
4 **J.G. Sample¹, J.B. Blake³, L.W. Blum², A.J. Halford²**

5 ¹Department of Physics, Montana State University, Bozeman, Montana, USA

6 ²NASA's Goddard Space Flight Center, Greenbelt, Maryland, USA

7 ³Space Science Applications Laboratory, The Aerospace Corporation, El Segundo, California USA

8 ⁴Johns Hopkins Applied Physics Laboratory, Laurel, Maryland, USA

9 **Key Points:**

- 10 • The dual AeroCube-6 CubeSats are used to identify stationary, narrow in latitude,
11 and persistent > 30 keV electron curtain precipitation.
12 • 90% of the observed curtains in Low Earth Orbit are narrower than 20 kilome-
13 ters in the latitudinal direction.
14 • Some curtains continuously precipitated into the atmosphere for multiple seconds.

Abstract

Curtain precipitation are a recently discovered stationary, persistent, and latitudinally narrow electron precipitation phenomenon in low Earth orbit. Curtains are observed over consecutive passes of the dual AeroCube-6 CubeSats while their in-track lag varied from a fraction of a second to 65 seconds, with dosimeters that are sensitive to > 30 keV electrons. This study uses the AeroCube-6 mission to quantify the statistical properties of 1,634 curtains observed over three years. We found that many curtains are narrower than 10 kilometers in the latitudinal direction with 90% narrower than 20 kilometers, corresponding to a few hundred kilometer radial size at the magnetic equator. We examined the magnetic local time and geomagnetic dependence of curtains. We found that curtains are observed in the late-morning and pre-midnight magnetic local times, with a higher occurrence rate at pre-midnight, and curtains are observed more often during times of enhanced Auroral Electrojet. We found a few curtains in the bounce loss cone region above the north Atlantic, whose electrons were continuously scattered for at least 6 seconds. Such observations suggest that continuous curtain precipitation may be a significant loss of > 30 keV electrons from the magnetosphere into the atmosphere, possibly scattered by a parallel direct current electric field.

Plain Language Summary

Electron curtain precipitation from space into Earth's atmosphere is a recently-discovered phenomenon observed by dual-spacecraft missions such as the AeroCube-6 CubeSats that orbit 700 kilometers above Earth's surface. Curtains appear stationary, remaining unchanged from seconds to a minute. Curtains are also very narrow along the satellite orbit that is mostly in the latitudinal direction. Besides these two properties, curtains and their impact on the magnetosphere and atmosphere are not well understood. Therefore, we used the AeroCube-6 mission, that took data together for three years, to statistically quantify curtain properties and to better understand their origin. We found 1,634 curtains and found that 90% of curtains are narrower than 20 kilometers in the latitudinal direction, curtains are observed on the outer radiation belt field lines predominately in the anti-sunward region, and curtains are observed when the magnetosphere is disturbed. Curtains observed in a special region above the North Atlantic shed light on their origin. A few dozen curtains observed in this North Atlantic region were continuously precipitating into the atmosphere for multiple seconds, and are unlikely to be drifting. Therefore, curtains may be a significant source of atmospheric ionization responsible for the natural depletion of ozone.

1 Introduction

Energetic particle precipitation into Earth's atmosphere plays a fundamental role in controlling the dynamics of Earth's radiation belts and ionization of Earth's upper atmosphere (e.g. Millan & Thorne, 2007; Randall et al., 2015). Even though particle precipitation, and its impact on the magnetosphere and the atmosphere, has been extensively studied since the 1960s, there are precipitation phenomena that are still poorly understood. One such form of precipitation that we have limited knowledge of are electron curtains.

Electron curtain precipitation is a stationary phenomenon observed in low Earth orbit (LEO). Curtains were recently discovered by Blake and O'Brien (2016) using the > 30 keV electron dosimeters onboard the dual AeroCube-6 (AC6) CubeSats that operated together between 2014 and 2017. Curtains are narrow in latitude and persist for up to a minute between subsequent satellite passes. This discovery was made possible by AC6's actively maintained in-track separation that varied between a few hundred meters and a few hundred kilometers. Besides the Blake and O'Brien (2016) study, not much is known about curtains including what they are, how are they generated, and their impact on the atmosphere. Answering these questions is an essential next step towards a

66 more complete understanding of how curtains, and particle precipitation in general, af-
67 fect the magnetosphere and Earth’s atmosphere.

68 In low Earth orbit, curtains are narrower than a few tens of kilometers in the lat-
69 itudinal direction. A polar-orbiting LEO satellite, such as AC6, will pass through the
70 curtain cross-section in a few seconds, which appears in the electron count time series
71 as short enhancements in flux. AC6 also observes similar-looking transient precipitation
72 called electron microbursts. Curtains and microbursts are observed in the AC6 data but
73 appear short-lived for different reasons: microbursts are temporal, while curtains are spa-
74 tial. Hence AC6, and other recently developed multi-spacecraft missions, are necessary
75 to identify and distinguish between transient microbursts and the persistent curtains.

76 Since the mid-1960s, microbursts have been observed by high altitude balloons where
77 they appear as sharp peaks in flux with a sub-second duration (e.g. Anderson & Mil-
78 ton, 1964; R. Brown et al., 1965; Parks, 1967). Because balloons are relatively station-
79 ary, a microburst is easily classified as a transient phenomenon. Microburst electrons have
80 also been directly observed by LEO satellites such as The Solar Anomalous and Mag-
81 netospheric Particle Explorer (e.g. Blake et al., 1996; Lorentzen, Blake, et al., 2001; O’Brien
82 et al., 2003; Douma et al., 2017). But a flux enhancement that looks like a microburst
83 from a single LEO satellite is ambiguous—it can be transient or it can be persistent, sta-
84 tionary, and narrow in latitude. Thus, multi-spacecraft missions such as the Focused In-
85 vestigations of Relativistic Electron Burst Intensity, Range, and Dynamics (FIREBIRD-
86 II) (Crew et al., 2016; Johnson et al., 2020) and AC6 (Blake & O’Brien, 2016; O’Brien
87 et al., 2016) are necessary to resolve the temporal vs. spatial ambiguity. While this study
88 focuses on curtain precipitation, microburst precipitation observed across the dawn sector
89 by AC6 was studied in Shumko et al. (2020).

90 While the impact of curtains on the magnetosphere and Earth’s atmosphere is un-
91 known, the impact of microbursts has been estimated to be substantial. Lorentzen, Looper,
92 and Blake (2001), Thorne et al. (2005), Breneman et al. (2017), and Douma et al. (2019),
93 among others, estimated that microbursts could deplete the outer radiation belt elec-
94 trons in about a day. Furthermore, Seppälä et al. (2018) modeled a 6-hour microburst
95 storm and concluded that microbursts depleted mesospheric ozone by roughly 10%. Mi-
96 crobursts and curtains can be easily misidentified from a single satellite; if curtains are
97 numerous, then the atmospheric and magnetospheric impact associated with microburst
98 observations from single satellites may be overestimated.

99 Precipitation bands, sometimes also referred to as spikes (e.g. Imhof et al., 1991),
100 are another form of precipitation that could be related to curtains. Precipitation bands
101 also appear as stationary and narrow flux enhancements with a > 1 second duration,
102 and can persist from an hour to as much as half a day (e.g. J. Brown & Stone, 1972; Blake
103 et al., 1996). Blum et al. (2013) identified two precipitation bands and estimated that
104 only 20 precipitation bands can deplete all of the outer radiation belt electrons. The mech-
105 anism responsible for scattering precipitation band electrons at high L is believed to be
106 field line curvature scattering, but the scattering mechanism for band electrons at lower
107 L shells is unknown. A few proposed scattering mechanisms include wave-particle inter-
108 actions and acceleration due to parallel direct current potentials (Hoffman & Evans, 1968).

109 Blake and O’Brien (2016) proposed a hypothesis that curtains are drifting remnants
110 of microbursts. If a microburst is not completely lost in the atmosphere after the ini-
111 tial scatter, the remaining microburst electrons will spread out (bounce phase disperse)
112 along the entire magnetic field line over a few bounce periods. Concurrently these elec-
113 trons drift to the east, with higher energy electrons drifting at a faster rate. Assuming
114 this hypothesis, the initially localized microburst is spread out in longitude into the shape
115 of a curtain. A similar phenomena was hypothesized by Lehtinen et al. (2000) who pre-
116 dicted that drifting curtains can be created by energetic runaway beams driven by light-
117 ning, but these curtains would be observed at relatively low L shells.

This study expands on Blake and O’Brien (2016) by examining the statistical properties of curtains. We use 1,634 confirmed curtain observations to study the distributions of the curtain: width in latitude, the geomagnetic conditions favorable to curtains, and the curtain distribution in L and magnetic local time (MLT). Lastly we will show examples of curtains that continuously precipitated in the bounce loss cone (BLC) region.

2 Instrumentation

The AC6 mission was a pair of 0.5U (10x10x5 cm) CubeSats built by The Aerospace Corporation and designed to measure the electron and proton environment in low Earth orbit (O’Brien et al., 2016). AC6 was launched on 19 June 2014 into a 620x700 km, 98° inclination orbit. The AC6 orbit over the three year mission lifetime was roughly dawn-dusk, and precessed only a few hours in MLT: 8-12 MLT in the dawn and 20-24 MLT in the dusk sectors. The two AC6 spacecraft, designated as AC6-A and AC6-B, separated after launch and were in proximity for the duration of the three-year mission—maintained by an active attitude control system. The attitude control system allowed them to actively control the amount of atmospheric drag experienced by each AC6 unit using the surface area of their solar panel “wings.” By changing their orientation, AC6 was able to maintain a separation between 2-800 km, confirmed by the Global Positioning System. The two AC6 units were in a string of pearls configuration, so one unit, typically unit A, was leading the other by an in-track lag: the time it would take the following spacecraft to catch up to the position of the leading spacecraft. To convert between the AC6 in-track separation and in-track lag, the AC6 orbital velocity was used. AC6’s orbital velocity was 7.6 km/s and varied by as much as 0.1 km/s. The in-track lag is readily available in the data files with the Global Positioning System, which makes it possible to remove the spatiotemporal ambiguity that affects single-spacecraft measurements.

Each AC6 unit contains three Aerospace microdosimeters (licensed to Teledyne Microelectronics, Inc) that measure the electron and proton dose in orbit (O’Brien et al., 2016). The dosimeter used for this study is dos1 with a > 30 keV integral electron response, as the other dosimeters either responded primarily to protons or were not identical between unit A and B. All dosimeters sample at 1 Hz in survey mode, and 10 Hz in burst mode. 10 Hz data is available from both AC6 units from June 2014 to May 2017 while their in-track lag was less than 65 seconds. Figure A1 in the appendix shows the distribution of 10 Hz data as a function of AC6 in-track lag.

3 Methodology

3.1 Curtain Identification

The 10 Hz data were used to identify curtains using the following two criteria: a high spatial correlation, and a prominent peak. Before we applied the identification criteria, the AC6-B time series was shifted by the in-track lag to spatially align it with the AC6-A time series.

The first identification criterion is a 1-second rolling Pearson correlation applied to both time series. Spatial features with a correlation greater than 0.8 are considered highly correlated. The second criterion is applied to the highly correlated features to check if they are also prominently peaked. To find peaked precipitation, we used a technique similar to the technique used by Blum et al. (2015) to identify precipitation bands, and by Greeley et al. (2019) to identify microbursts. Our technique quantified the number of Poisson standard deviations, σ , that dos1 counts in each 100 ms bin are above a 10-second centered running average, b_{10} . Locations where dos1 counts are at least two σ above b_{10} , in other words $dos1 > 2\sqrt{b_{10}} + b_{10}$, are considered prominently peaked. One bias inherent to this detection algorithm, and similar algorithms such as the burst parameter (O’Brien et al., 2003), is a reduced sensitivity for wider peaks. For curtains with

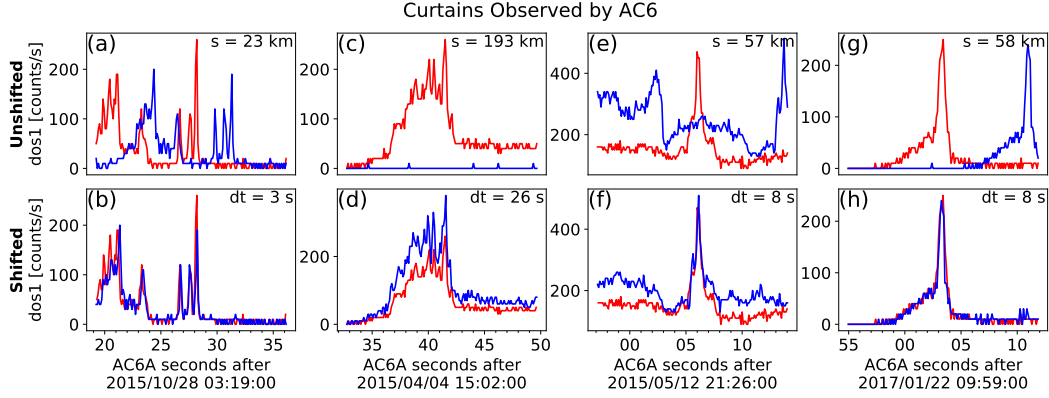


Figure 1. Four examples showing the > 30 keV electron time series data taken by AC6 at the same time (unshifted) in the top row and at the same position (shifted by dt seconds) in the bottom row. AC6-A, whose data is shown with the red curves, was s kilometers ahead of AC6-B. To show the data at the same position the AC6-B time series was shifted by the in-track lag annotated by dt . These examples show that curtain precipitation was highly correlated for up to 26 seconds.

167 a width similar to b_{10} , the baseline will be significantly elevated making the curtain peak
 168 less pronounced.

169 We tuned the automated detection parameters to identify a large number of curtains.
 170 Once curtains were automatically identified, one author visually inspected 6,149
 171 candidate curtains and verified 1,634 curtains. The visual inspection was performed to
 172 remove ambiguous detections where the peaks lined up in space and time, and false positive
 173 detections that were triggered by three conditions: sharp count rate shoulders, low
 174 baseline (b_{10}), and high correlations resulting from Poisson noise. Four curtain exam-
 175 ples are shown in Fig. 1. In each instance, the unmodified time series is shown in the
 176 top row and the spatially-aligned time series in the bottom row. The in-track lag used
 177 to shift the bottom row is annotated by dt , corresponding to an AC6 in-track separa-
 178 tion annotated by s . The bottom row shows highly correlated curtains observed at the
 179 same location for at least 3 to 26 seconds.

180 3.2 Differentiating Between Drifting and Precipitating Curtains

181 The AC6 dosimeters lack the necessary pitch angle resolution to differentiate between
 182 locally drifting and precipitating electrons to test the Blake and O'Brien (2016)
 183 hypothesis that curtains are the drifting remnants of microbursts. Fortunately, one stan-
 184 dard method of distinguishing between locally precipitating, drifting, and trapped par-
 185 ticles is by using the geographic location of observations with respect to the location of
 186 the South Atlantic Anomaly (SAA).

187 Earth's magnetic field is asymmetric and has a region of weaker magnetic field in
 188 the South Atlantic Ocean called the South Atlantic Anomaly. The weaker magnetic field
 189 in the SAA naturally differentiates particles by pitch angle into trapped and quasi-trapped
 190 populations. While some particles observed in LEO are trapped and will execute closed
 191 drift paths, most particles observed in LEO are quasi-trapped: they drift around the Earth
 192 until they reach the SAA. Within the SAA, the weaker magnetic field strength can lower
 193 the particle's mirror point altitude into the atmosphere, where collisions with the atmo-
 194 spheric neutrals and ions are more numerous and the particle is lost.

195 Particles that are quasi-trapped have pitch angles in the drift loss cone and will pre-
 196 cipitate within one drift period (often within the SAA). Particles with smaller equato-
 197 rial pitch angles that are lost in the atmosphere within one bounce are in the bounce loss
 198 cone (BLC). Traditionally, a particle is in the BLC if its mirror point altitude is at or
 199 below 100 km in either hemisphere (e.g. Selesnick et al., 2003).

200 In most regions outside of the SAA and its conjugate point in the North Atlantic,
 201 AC6 will observe a combination of drift and bounce loss cone electrons. In the SAA, AC6
 202 does not only observe electrons that are immediately lost, but a combination of electrons
 203 that are in the drift loss cone, bounce loss cone, and trapped (a trapped electron that
 204 locally mirrors at AC6’s altitude in the SAA will mirror at higher altitudes everywhere
 205 else). In the region magnetically conjugate to the SAA in the North Atlantic, AC6 only
 206 observes electrons in the BLC. Here, if an electron makes it to AC6’s altitude, it might
 207 be in the local loss cone and precipitate in the local hemisphere. Alternatively, the elec-
 208 tron may mirror at or below AC6 and bounce to its conjugate mirror point deep in the
 209 atmosphere or below sea level in the SAA. Therefore, any electrons observed in the BLC
 210 region will likely precipitate within one bounce (≈ 1.5 seconds for 30 keV electrons).

211 We estimated the BLC region for locally-mirroring electrons in the North Atlantic
 212 Ocean using the IRBEM-Lib magnetic field library and the Olson-Pfitzer magnetic field
 213 model (Boscher et al., 2012; Olson & Pfitzer, 1982). We defined a latitude-longitude grid,
 214 with a $\approx 0.5^\circ \times 0.5^\circ$ grid size, spanning the North Atlantic at 700-kilometers altitude,
 215 and estimated the local magnetic field strength. The 700-kilometers altitude was cho-
 216 sen because it is the upper bound altitude for AC6’s orbit and it is the conservative limit
 217 because at lower altitudes the BLC region is larger. For each latitude-longitude point
 218 we traced the magnetic field line to the southern hemisphere and found the conjugate
 219 mirror point altitude. If the conjugate mirror point is ≤ 100 kilometers, the electron is
 220 likely lost and the associated grid point is in the BLC. Furthermore, a more rigorous bounce
 221 loss cone criterion is the conjugate mirror point altitude below sea level. In this case, the
 222 electron is very likely lost. The BLC region estimated by this method closely matches
 223 the BLC region shown in Comess et al. (2013, Figure 1) and Dietrich et al. (2010, Fig-
 224 ure 3) for other LEO satellites. Lastly, we repeated the same analysis using the Tsyga-
 225 nenko 1989 model (Tsyganenko, 1989), which yielded similar BLC boundaries.

226 4 Results

227 In this study we addressed three questions: what is the distribution of curtain widths
 228 along the AC6 orbit (mostly in geographic latitude), when and where are curtains ob-
 229 served, and are curtains composed of drifting or locally precipitating electrons?

230 4.1 Curtain Width

231 The curtain width is quantified as the width at half of the curtain’s topographic
 232 prominence, as described in Appendix B. The spatial width of a curtain is then the prod-
 233 uct of the observed width in time and AC6’s orbital velocity. The curtain width is mea-
 234 sured along AC6’s orbit track which is mostly in the latitudinal direction, therefore the
 235 estimated curtain widths are also mostly in the latitudinal direction. The distribution
 236 of curtain widths is shown in Fig. 2. Curtains are very narrow. Many curtains are nar-
 237 rower than 10 km in the latitudinal direction, and 90% are narrower than 20 km.

238 4.2 When and Where Are Curtains Observed

239 The distribution of curtains in L and MLT is shown in Fig. 3. Figure 3a shows the
 240 distribution of the observed curtains, while Fig. 3b shows the same distribution normal-
 241 ized by the number of quality 10 Hz samples (flag = 0 in the data files) that both AC6
 242 spacecraft took at the same location in each L-MLT bin. In Fig. 3a and 3b, the bins where

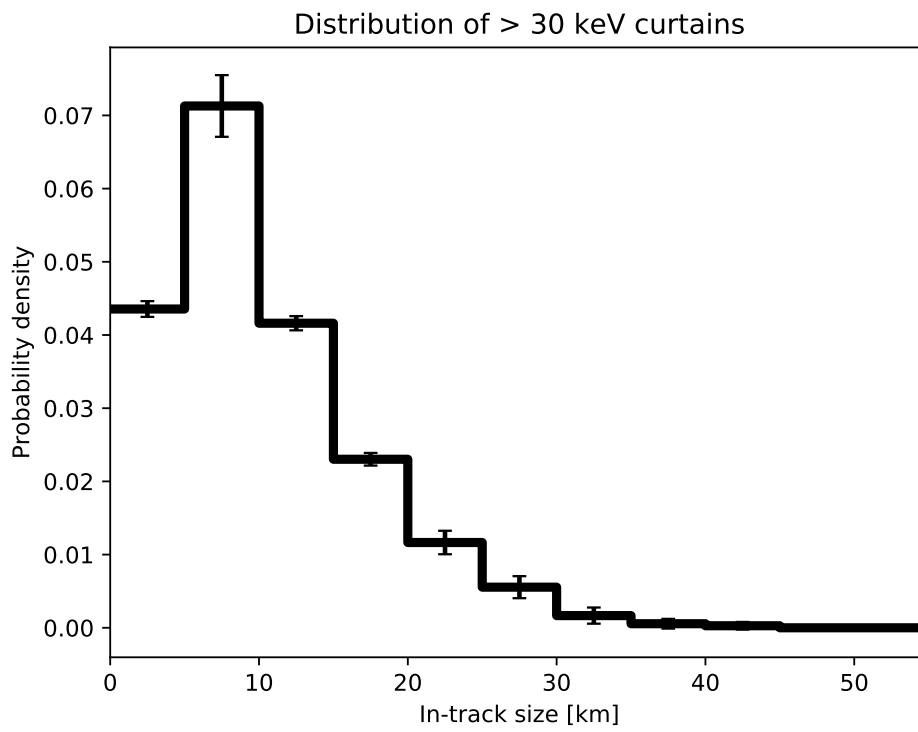


Figure 2. The distribution of curtain widths along the AC6 orbit. The error bars are derived assuming the Poisson standard error.

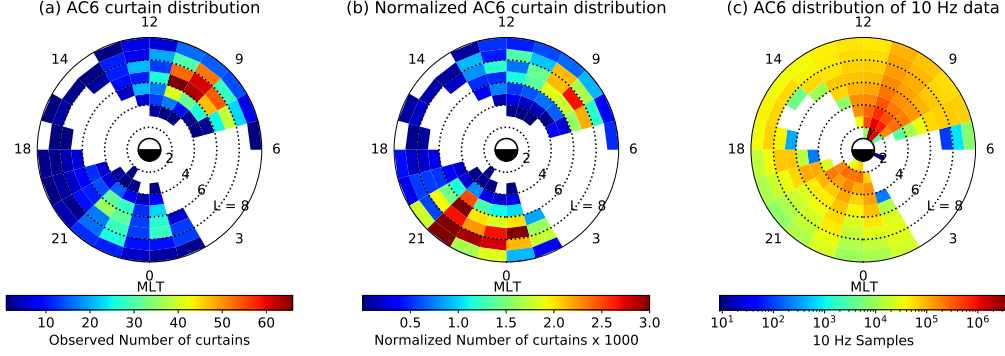


Figure 3. The distribution of observed curtains by L shell and MLT. Panel a shows the locations of all observed curtains used in this study. Panel b shows the curtain distribution normalized by the number of quality 10 Hz samples taken in each bin, shown in panel c. The white bins in panels a and b show where no curtains were observed, while in panel c the white bins show where AC6 did not take any 10 Hz data at the same location.

no curtains were observed are white. The AC6 sampling distribution is shown in Fig. 3c, whose white bins show where AC6 did not take any 10 Hz data at the same location. The normalized curtain distribution in Fig. 3b shows an enhanced curtain occurrence in the outer radiation belt ($L \approx 5-8$) with the largest peak in the pre-midnight MLT sector.

We also examine the geomagnetic conditions favorable for curtains. Figure 4a shows the distribution of the minute cadence Auroral Electroject (AE) index between 2014 and 2017 in solid black, for times when quality 10 Hz data were available from both AC6 units. Furthermore, the distribution of the AE index when curtains were observed is shown by the solid blue lines. Curtains are observed during both low and high geomagnetic activity, slightly more often at higher AE than the index itself (curtain distribution trends above the AE index when $AE > 200$). Lastly, we normalized the curtain distribution in Fig. 4a assuming any AE index is equally probable. The normalized curtain distribution is shown in Fig. 4b, which emphasizes that the curtain occurrence frequency increases with increasing AE index up to ≈ 600 nT.

4.3 Local Atmospheric Precipitation

Lastly, we investigate if curtains are drifting or locally precipitating. Figure 5a shows a map of the northern BLC region in the North Atlantic. The solid blue line is the northern boundary where an electron that mirrors locally at 700 km has a conjugate mirror point at 100 km in the SAA. Immediately south of the solid blue line, the conjugate mirror altitude rapidly decreases towards, and below, sea level. The dashed blue line is the boundary where the conjugate mirror point altitude is at sea level. South of this line the conjugate mirror point is inside the Earth. For reference, AC6 takes about 30 seconds to move between the solid and dashed blue curves. The two dotted black curves in Fig. 5a are roughly the boundary of the outer radiation belt, defined as $L = 4 - 8$.

Of the 1,634 curtains, we found 36 curtains that were observed inside the BLC region. Figure 5b-e shows 4 curtain examples (AC6-B time shifted by the in-track lag), along with the AC6 in-track lag, L and MLT during the observations annotated. The AC6 locations where these curtains were observed are shown in Fig. 5a with the red stars and the corresponding panel labels.

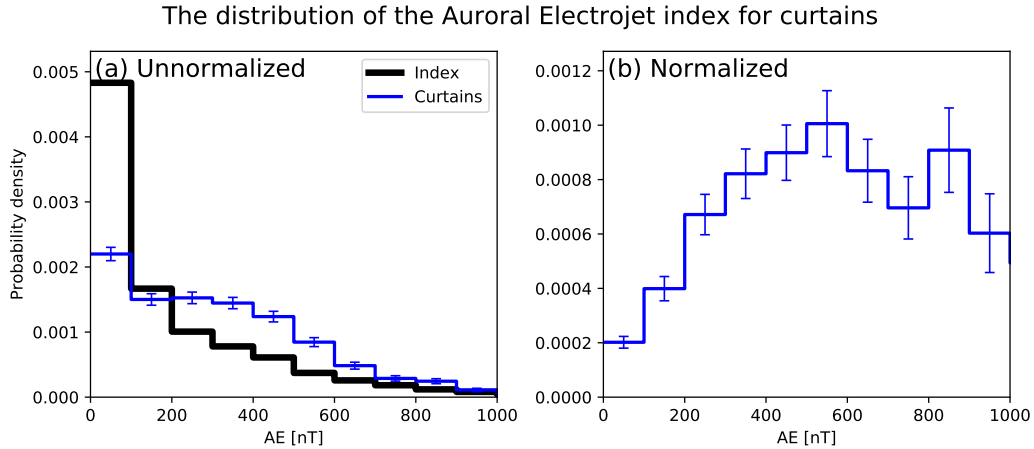


Figure 4. The distribution of the Auroral Electrojet (AE) index when curtains were observed. The blue line in panel a shows the distribution of AE when curtains were observed, and for reference the black line shows the distribution of the AE index between 2014 and 2017 when quality 10 Hz data is available from both AC6 spacecraft. Panel b shows the curtain distribution normalized by the AE index distribution, and it represents the distribution assuming that any AE index is equally probable. The error bars are derived assuming the Poisson standard error.

5 Discussion

5.1 Curtain Width

Curtains are narrow in latitude. Figure 2 shows that the width of most curtains is on the order of 1–3 seconds in time as observed by AC6, corresponding to a 8–20 kilometer spatial width along the AC6 orbit track. The reduced sensitivity of the detection algorithm, as described in Section 3.1, is unlikely to significantly underestimate the curtain width distribution because most curtains had a width less than half of the 10-second baseline’s width. Scaled to the magnetic equator, the curtain widths correspond to a source with a radial scale size of a few hundred kilometers. The curtains with a < 1 second duration suggest that past microburst observations could have been mistaken for curtains, so the microburst impact on the atmosphere and the radiation belt is overestimated.

As shown in Fig. 1, it is remarkable that some curtains maintain a fine structure after multiple seconds with little observable difference. However, sometimes curtains appear to be slightly and systematically shifted in latitude, while maintaining their fine structure (not shown).

5.2 When and Where Are Curtains Observed

Figure 3b shows that curtains likely originate in the outer radiation belt and are observed relatively more in the pre-midnight than late-morning MLT regions. Furthermore, curtains are more often observed at higher L shells near midnight MLT, however the sampling statistics at high L are limited because AC6 rapidly crosses high L shells. Nevertheless, Fig. 3b hints that curtains near midnight MLT were observed at L shells possibly outside the outer radiation belt. Lastly, Figure 4b shows that curtains are associated with an enhanced AE up to around 600 nT. While it is not a direct comparison (due to the electron energy channels and the binning scheme), Douma et al. (2019)

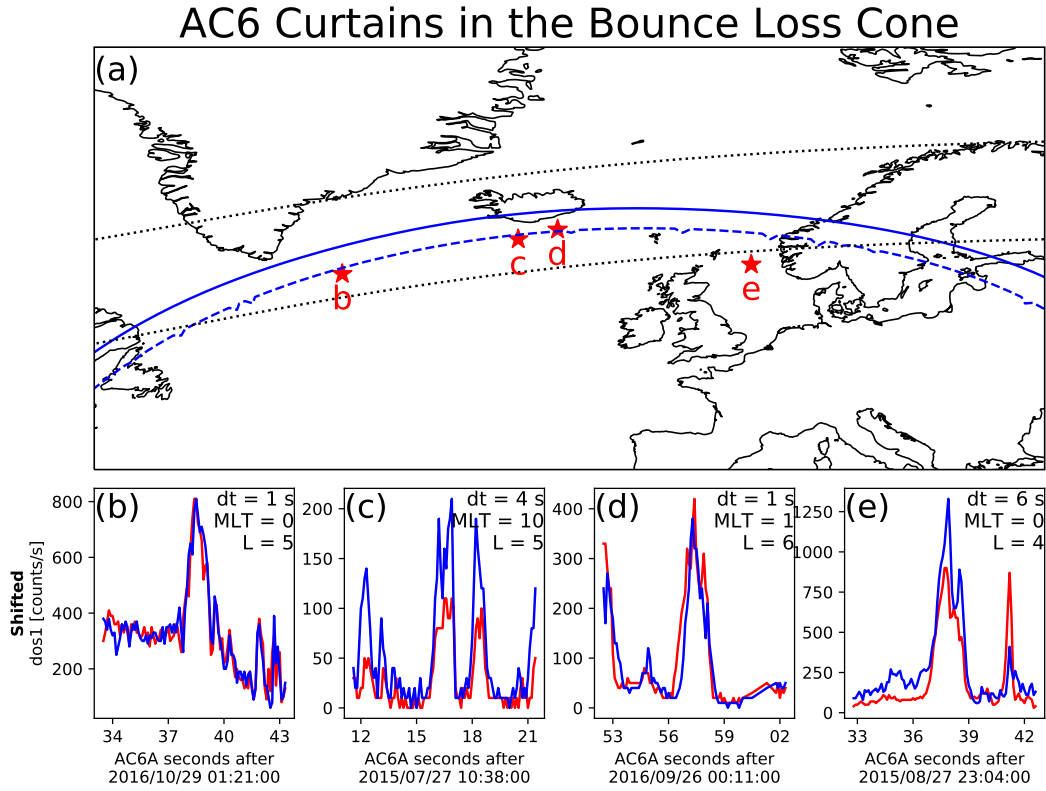


Figure 5. Curtains observed in the bounce loss cone region. Panel a shows a map of the North Atlantic region with the outer radiation belt, defined by $L = 4 - 8$, shown with the dotted black curves. The solid blue curve shows the northern boundary of the bounce loss cone region. Along this curve, electrons locally mirroring at 700 kilometers altitude have a conjugate mirror point at 100 kilometers altitude in the SAA. A more strict bounce loss cone criterion is the dashed blue curve that represents a conjugate mirror point altitude at sea level in the SAA. The 4 red stars with labels show the locations of the curtain examples shown in the corresponding panels b-e. The panels b-e show the 4 example curtains with the AC6-A data shown by the red line and the time-shifted AC6-B data with the blue line. The annotations in each example show the AC6 in-track lag (dt), L , and MLT rounded to the nearest integer. AC6-A was leading in all examples except in panel d.

298 showed that the number of microburst observed by SAMPEX increases with increasing
299 AE, up to about AE = 300 nT.

300 5.3 Curtains Observed in The Bounce Loss Cone

301 The handful of curtains observed in the bounce loss cone, and shown in Fig. 5, put
302 the Blake and O'Brien (2016) curtain drift hypothesis into question. These curtains were
303 observed near the sea level mirror altitude curve. One possible explanation is that the
304 drifting curtain electrons were observed at the end of their drift orbit, however because
305 these examples were seen far from the western edge of the BLC, any drifting electrons
306 would have been lost before AC6 observed them. Thus, they were not drifting and were
307 precipitating for as long as 6 seconds, as shown in Fig. 5e. The curtain precipitation per-
308 sisted for multiple bounce periods (≈ 1.5 seconds for 30 keV electrons in this region),
309 suggesting that the curtain generation mechanism must be capable of persistently scat-
310 tering electrons. The scattering mechanism must be radially localized; if we assume the
311 mechanism is at the magnetic equator, it must be on a scale of a few hundred kilome-
312 ters.

313 One candidate mechanism is a direct current electric field that is parallel to the back-
314 ground magnetic field that lowers the electron mirror point to AC6 altitudes. To find
315 the minimum potential we assume the electron is barely trapped and has a 100-kilometer
316 conjugate mirror point altitude in the SAA, so initially the electron will mirror above
317 AC6 in the bounce loss cone region.

318 To find the parallel potential, $q\Phi$, we use the kinetic energy, W , of a 30 keV elec-
319 tron at its initial mirror point with a magnetic field strength of B_i . The kinetic energy
320 at the initial mirror point can be written as $W_i = \mu B_i$ where μ is the first adiabatic
321 invariant that is conserved during this acceleration. When a parallel potential acceler-
322 ates the electron of charge q and does $q\Phi$ amount of work, the electron will mirror closer
323 to Earth's surface and mirror at a field strength B_f where its final energy is $W_f = \mu B_f$.
324 Now we relate the initial and final kinetic energy of the electron,

$$\mu B_f = \mu B_i + q\Phi. \quad (1)$$

325 Then we solve for $q\Phi$ and substitute μ to express the above equation as a function of the
326 initial kinetic energy

$$q\Phi = W_i \frac{(B_f - B_i)}{B_i}. \quad (2)$$

327 The parallel potential is proportional to W_i so a larger potential is necessary to accel-
328 erate higher energy electrons. AC6 dos1 electron energy response increases rapidly from
329 30 keV to a peak at 100 keV (Figure 2 in O'Brien et al., 2019), therefore our assump-
330 tion that $W_i = 30$ keV can underestimate the parallel potential. Nevertheless, the counts
331 observed by AC6 are a convolution of, among other things, the AC6 dos1 electron en-
332 ergy response and the falling electron energy spectrum. Thus, the majority of electrons
333 that AC6 observed have energies close to 30 keV and the $W_i = 30$ keV is an appropri-
334 ate approximation.

335 We again used IRBEM-Lib to estimate $q\Phi$. For each example curtain in Fig. 5, we
336 first estimated the local magnetic field, B_f , that the electron descended to after the ac-
337 celeration. Then we traced the local field line into the SAA. We estimated B_i at 100 kilo-
338 meters altitude in the SAA for barely trapped electrons. With the initial and final B ,
339 along with $W = 30$ keV, the minimum potential was between $q\Phi = 1 - 4$ kV for the
340 examples shown in Fig. 5.

341 The range of estimated potentials is typical for the inverted-V discrete aurora. Partamies
 342 et al. (2008), using observations made by the Fast Auroral SnapshoT (FAST) mission,
 343 reported that auroral inverted-V electron precipitation structures, with electron ener-
 344 gies up to a few tens of keV, were accelerated by 2-4 kV parallel potentials. The inverted-
 345 V structure and curtains share several similarities including: latitudinal width, high oc-
 346 currence rate in the midnight MLT region, and the maximum inverted-V energy extends
 347 into tens of keV (e.g. Marklund et al., 2011; Thieman & Hoffman, 1985). AC6’s dos1,
 348 with its 30 keV electron threshold, may by observing the highest energy tip of the inverted-
 349 V aurora. A possible connection between the inverted-V structures is intriguing, but by
 350 itself AC6 cannot easily test this hypothesis. To investigate further, a follow-on study
 351 could look at ground-based auroral imager data and look for meso-scale auroral arcs when
 352 AC6 observed curtains overhead.

353 Regardless of the source of the curtain precipitation, the impact of curtains on the
 354 atmosphere needs to be quantified. Even if the curtains observed in the BLC are the ex-
 355 ception and other curtains are drifting, the drifting curtains will still precipitate within
 356 one drift period. Precipitating electrons produce odd reactive nitrogen (NO_x) molecules
 357 that are currently underestimated by atmospheric models such as the widely-used Whole
 358 Atmosphere Community Climate Model (WACCM) (e.g. Randall et al., 2015). Curtain
 359 precipitation could explain the lack of atmospheric NO_x . An AC6-like mission with pitch
 360 angle and energy resolution will be necessary to quantify the curtain impact on the at-
 361 mosphere.

362 6 Conclusions

363 The 1,634 curtains examined here allowed us to make the following inferences:

- 364 1. Curtains are narrow—90% are less than 20 kilometers wide in the latitudinal di-
 365 rection.
- 366 2. Curtains are observed predominately in the pre-midnight MLT region, and dur-
 367 ing active geomagnetic periods.
- 368 3. Some curtains continuously precipitate into the atmosphere for multiple seconds.

369 As shown in Fig. 1, curtain precipitation is narrow with a fine structure that per-
 370 sists for multiple seconds: for at least 26 seconds as shown in Fig. 1d. Either the scat-
 371 tering mechanism that continuously generates curtains is physically static for multiple
 372 seconds, or the curtain electron drift is often undisturbed.

373 The curtain-microburst relationship hypothesized in Blake and O’Brien (2016) is
 374 not clear. Curtains observed in the bounce loss cone cast doubt on the curtain-microburst
 375 hypothesis. Some curtains continuously precipitate for at least a few seconds, and can
 376 be a significant source of energetic electron precipitation into the atmosphere. Lastly,
 377 we found that the continuous scattering of curtain electrons can be explained by a par-
 378 allel direct current electric field, possibly relating curtains to the aurora.

379 Appendix A Distribution of Colocated 10 Hz Data

380 Figure A1 shows the distribution of colocated AC6 10 Hz data as a function of in-
 381 track lag. This distribution is heavily dominated by small in-track lags and 72% of the
 382 colocated 10 Hz data was taken when AC6 was separated in-track by less than 10 sec-
 383 onds, corresponding to 75 km in-track separation. Therefore, most of the curtains stud-
 384 ied here were observed for small in-track lags, which limits our ability to explore the ex-
 385 tent of the curtain duration.

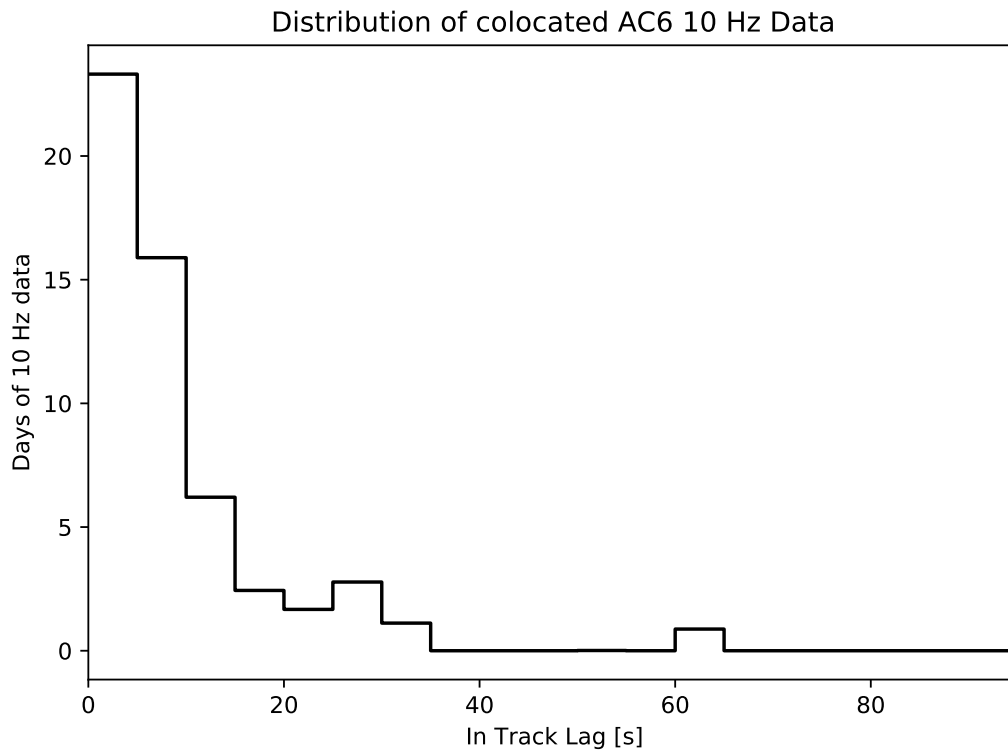


Figure A1. The distribution of colocated 10 Hz data as a function of in-track lag. Bins are 5 kilometers wide.

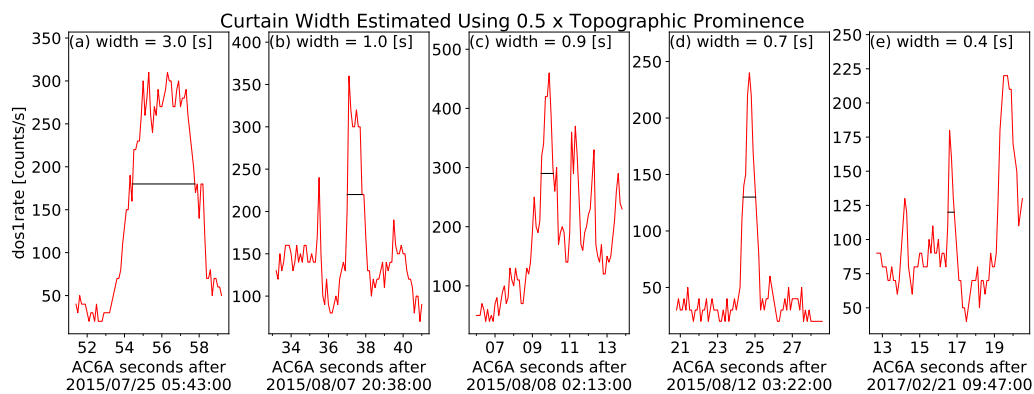


Figure B1. Five examples of curtains observed by AC6A shown with the red curves and the curtain widths are shown with the horizontal black lines and annotated. The height of the horizontal black lines are at half of the curtain's topographic prominence.

Appendix B Estimating Curtain Widths

The curtain width in the dos1 time series is defined here as the width at half of the curtain's topographic prominence. Topographic prominence for a peak in a time series is the height of a peak relative to the maximum of the two minima on either side of the peak. The minima on either side of the peak are searched for between the peak and the nearest higher peak on that side. Figure B1 shows 5 examples of curtains observed by AC6-A in red (for clarity the AC6-B data is not shown), and the curtain width is shown by the horizontal black line.

Acknowledgments

This work was made possible with the help from the many engineers and scientists at The Aerospace Corporation who designed, built, and operated AC6. M. Shumko was supported by NASA Headquarters under the NASA Earth and Space Science Fellowship Program - Grant 80NSSC18K1204 and NASA Postdoctoral Program at the NASA's Goddard Space Flight Center, administered by Universities Space Research Association under contract with NASA. D.L. Turner is thankful for funding from a NASA grant (prime award #: 80NSSC19K0280). The work at The Aerospace Corporation was supported in part by RBSP-ECT funding provided by JHU/APL contract 967399 under NASA's Prime contract NAS501072. The AC6 data and documentation is available at <http://rbspqway.jhuapl.edu/ac6> and the IRBEM-Lib version used for this analysis can be downloaded from <https://sourceforge.net/p/irbem/code/616/tree/>.

References

- Anderson, K. A., & Milton, D. W. (1964). Balloon observations of X rays in the auroral zone: 3. High time resolution studies. *Journal of Geophysical Research*, 69(21), 4457–4479. Retrieved from <http://dx.doi.org/10.1029/JZ069i021p04457> doi: 10.1029/JZ069i021p04457
- Blake, J. B., Looper, M. D., Baker, D. N., Nakamura, R., Klecker, B., & Hovestadt, D. (1996). New high temporal and spatial resolution measurements by sampex of the precipitation of relativistic electrons. *Advances in Space Research*, 18(8), 171 - 186. Retrieved from <http://www.sciencedirect.com/science/article/pii/0273117795009698> doi: [http://dx.doi.org/10.1016/0273-1177\(95\)00969-8](http://dx.doi.org/10.1016/0273-1177(95)00969-8)

- 417 Blake, J. B., & O'Brien, T. P. (2016). Observations of small-scale latitudinal struc-
 418 ture in energetic electron precipitation. *Journal of Geophysical Research: Space*
 419 *Physics*, *121*(4), 3031–3035. Retrieved from [http://dx.doi.org/10.1002/](http://dx.doi.org/10.1002/2015JA021815)
 420 [2015JA021815](http://dx.doi.org/10.1002/2015JA021815) (2015JA021815) doi: 10.1002/2015JA021815
- 421 Blum, L., Li, X., & Denton, M. (2015). Rapid MeV electron precipitation as ob-
 422 served by SAMPEX/HILT during high-speed stream-driven storms. *Jour-*
 423 *nal of Geophysical Research: Space Physics*, *120*(5), 3783–3794. Retrieved
 424 from <http://dx.doi.org/10.1002/2014JA020633>
 425 (2014JA020633) doi: 10.1002/2014JA020633
- 426 Blum, L., Schiller, Q., Li, X., Millan, R., Halford, A., & Woodger, L. (2013). New
 427 conjunctive cubesat and balloon measurements to quantify rapid energetic
 428 electron precipitation. *Geophysical research letters*, *40*(22), 5833–5837.
- 429 Boscher, D., Bourdarie, S., O'Brien, P., Guild, T., & Shumko, M. (2012). *Irbem-lib*
 430 *library*.
- 431 Breneman, A., Crew, A., Sample, J., Klumpar, D., Johnson, A., Agapitov, O., ...
 432 others (2017). Observations directly linking relativistic electron microbursts
 433 to whistler mode chorus: Van allen probes and FIREBIRD II. *Geophysical*
 434 *Research Letters*.
- 435 Brown, J., & Stone, E. (1972). High-energy electron spikes at high latitudes. *Journal*
 436 *of Geophysical Research*, *77*(19), 3384–3396.
- 437 Brown, R., Barcus, J., & Parsons, N. (1965, 6). Balloon observations of auroral zone
 438 x rays in conjugate regions. 2. microbursts and pulsations. *Journal of Geophys-*
 439 *ical Research (U.S.)*, *70*. doi: 10.1029/JZ070i011p02599
- 440 Comess, M., Smith, D., Selesnick, R., Millan, R., & Sample, J. (2013). Duskside
 441 relativistic electron precipitation as measured by sampex: A statistical sur-
 442 vey. *Journal of Geophysical Research: Space Physics*, *118*(8), 5050-5058.
 443 Retrieved from [https://agupubs.onlinelibrary.wiley.com/doi/abs/](https://agupubs.onlinelibrary.wiley.com/doi/abs/10.1002/jgra.50481)
 444 [10.1002/jgra.50481](https://agupubs.onlinelibrary.wiley.com/doi/abs/10.1002/jgra.50481) doi: 10.1002/jgra.50481
- 445 Crew, A. B., Spence, H. E., Blake, J. B., Klumpar, D. M., Larsen, B. A., O'Brien,
 446 T. P., ... Widholm, M. (2016). First multipoint in situ observations of elec-
 447 tron microbursts: Initial results from the NSF FIREBIRD II mission. *Jour-*
 448 *nal of Geophysical Research: Space Physics*, *121*(6), 5272–5283. Retrieved
 449 from <http://dx.doi.org/10.1002/2016JA022485>
 450 (2016JA022485) doi: 10.1002/2016JA022485
- 451 Dietrich, S., Rodger, C. J., Clilverd, M. A., Bortnik, J., & Raita, T. (2010). Rela-
 452 tivistic microburst storm characteristics: Combined satellite and ground-based
 453 observations. *Journal of Geophysical Research: Space Physics*, *115*(A12).
- 454 Douma, E., Rodger, C., Blum, L., O'Brien, T., Clilverd, M., & Blake, J. (2019).
 455 Characteristics of relativistic microburst intensity from sampex observations.
 456 *Journal of Geophysical Research: Space Physics*.
- 457 Douma, E., Rodger, C. J., Blum, L. W., & Clilverd, M. A. (2017). Occurrence
 458 characteristics of relativistic electron microbursts from SAMPEX observations.
 459 *Journal of Geophysical Research: Space Physics*, *122*(8), 8096–8107. Retrieved
 460 from <http://dx.doi.org/10.1002/2017JA024067>
 461 (2017JA024067) doi: 10.1002/2017JA024067
- 462 Greeley, A., Kanekal, S., Baker, D., Klecker, B., & Schiller, Q. (2019). Quantifying
 463 the contribution of microbursts to global electron loss in the radiation belts.
 464 *Journal of Geophysical Research: Space Physics*.
- 465 Hoffman, R. A., & Evans, D. S. (1968). Field-aligned electron bursts at high lati-
 466 tudes observed by ogo 4. *Journal of Geophysical Research*, *73*(19), 6201–6214.
- 467 Imhof, W., Voss, H., Mabilia, J., Datlowe, D., & Gaines, E. (1991). The precipita-
 468 tion of relativistic electrons near the trapping boundary. *Journal of Geophys-*
 469 *ical Research: Space Physics*, *96*(A4), 5619–5629.
- 470 Johnson, A., Shumko, M., Griffith, B., Klumpar, D., Sample, J., Springer, L., ...
 471 others (2020). The FIREBIRD-II CubeSat mission: Focused investigations of

- 472 relativistic electron burst intensity, range, and dynamics. *Review of Scientific*
 473 *Instruments*, 91(3), 034503.
- 474 Lehtinen, N. G., Inan, U. S., & Bell, T. F. (2000). Trapped energetic electron
 475 curtains produced by thunderstorm driven relativistic runaway electrons. *Geo-*
 476 *physical research letters*, 27(8), 1095–1098.
- 477 Lorentzen, K. R., Blake, J. B., Inan, U. S., & Bortnik, J. (2001). Observations of
 478 relativistic electron microbursts in association with VLF chorus. *Journal of*
 479 *Geophysical Research: Space Physics*, 106(A4), 6017–6027. Retrieved from
 480 <http://dx.doi.org/10.1029/2000JA003018> doi: 10.1029/2000JA003018
- 481 Lorentzen, K. R., Looper, M. D., & Blake, J. B. (2001). Relativistic electron mi-
 482 crobursts during the GEM storms. *Geophysical Research Letters*, 28(13),
 483 2573–2576. Retrieved from <http://dx.doi.org/10.1029/2001GL012926> doi:
 484 10.1029/2001GL012926
- 485 Marklund, G. T., Sadeghi, S., Cumnock, J. A., Karlsson, T., Lindqvist, P.-A.,
 486 Nilsson, H., ... others (2011). Evolution in space and time of the quasi-
 487 static acceleration potential of inverted-v aurora and its interaction with
 488 alfvénic boundary processes. *Journal of Geophysical Research: Space Physics*,
 489 116(A1).
- 490 Millan, R., & Thorne, R. (2007). Review of radiation belt relativistic electron
 491 losses. *Journal of Atmospheric and Solar-Terrestrial Physics*, 69(3), 362 -
 492 377. Retrieved from [//www.sciencedirect.com/science/article/pii/](http://www.sciencedirect.com/science/article/pii/S1364682606002768)
 493 [S1364682606002768](http://www.sciencedirect.com/science/article/pii/S1364682606002768) doi: <http://dx.doi.org/10.1016/j.jastp.2006.06.019>
- 494 O'Brien, T. P., Blake, J. B., & W., G. J. (2016, May). *AeroCube-6 dosimeter data*
 495 *README* (Tech. Rep. No. TOR-2016-01155). The Aerospace Corporation.
- 496 O'Brien, T. P., Looper, M. D., & Blake, J. B. (2019, July). *AeroCube-6 dosime-*
 497 *ter equivalent energy thresholds and flux conversion factors* (Tech. Rep. No.
 498 TOR-2017-02598). The Aerospace Corporation.
- 499 O'Brien, T. P., Lorentzen, K. R., Mann, I. R., Meredith, N. P., Blake, J. B., Fen-
 500 nell, J. F., ... Anderson, R. R. (2003). Energization of relativistic elec-
 501 trons in the presence of ULF power and MeV microbursts: Evidence for dual
 502 ULF and VLF acceleration. *Journal of Geophysical Research: Space Physics*,
 503 108(A8). Retrieved from <http://dx.doi.org/10.1029/2002JA009784> doi:
 504 10.1029/2002JA009784
- 505 Olson, W. P., & Pfitzer, K. A. (1982). A dynamic model of the magnetospheric
 506 magnetic and electric fields for July 29, 1977. *Journal of Geophysical Research:*
 507 *Space Physics*, 87(A8), 5943–5948. Retrieved from [http://dx.doi.org/](http://dx.doi.org/10.1029/JA087iA08p05943)
 508 [10.1029/JA087iA08p05943](http://dx.doi.org/10.1029/JA087iA08p05943) doi: 10.1029/JA087iA08p05943
- 509 Parks, G. K. (1967). Spatial characteristics of auroral-zone X-ray microbursts. *Jour-*
 510 *nal of Geophysical Research*, 72(1), 215–226.
- 511 Partamies, N., Donovan, E., & Knudsen, D. (2008). Statistical study of inverted-v
 512 structures in fast data. In *Annales geophysicae* (Vol. 26, pp. 1439–1449).
- 513 Randall, C. E., Harvey, V. L., Holt, L. A., Marsh, D. R., Kinnison, D., Funke, B.,
 514 & Bernath, P. F. (2015). Simulation of energetic particle precipitation effects
 515 during the 2003–2004 arctic winter. *Journal of Geophysical Research: Space*
 516 *Physics*, 120(6), 5035–5048.
- 517 Selesnick, R. S., Blake, J. B., & Mewaldt, R. A. (2003). Atmospheric losses of radi-
 518 ation belt electrons. *Journal of Geophysical Research: Space Physics*, 108(A12).
 519 Retrieved from <http://dx.doi.org/10.1029/2003JA010160> (1468) doi: 10
 520 .1029/2003JA010160
- 521 Seppälä, A., Douma, E., Rodger, C., Verronen, P., Clilverd, M. A., & Bortnik, J.
 522 (2018). Relativistic electron microburst events: Modeling the atmospheric
 523 impact. *Geophysical Research Letters*, 45(2), 1141–1147.
- 524 Shumko, M., Johnson, A., Sample, J., Griffith, B. A., Turner, D. L., O'Brien, T. P.,
 525 ... Claudepierre, S. G. (2020). Electron microburst size distribution de-
 526 rived with AeroCube-6. *Journal of Geophysical Research: Space Physics*,

- 527 e2019JA027651.
- 528 Thieman, J. R., & Hoffman, R. A. (1985). Determination of inverted-v stability
529 from dynamics explorer satellite data. *Journal of Geophysical Research: Space*
530 *Physics*, *90*(A4), 3511–3516.
- 531 Thorne, R. M., O’Brien, T. P., Shprits, Y. Y., Summers, D., & Horne, R. B. (2005).
532 Timescale for MeV electron microburst loss during geomagnetic storms. *Jour-*
533 *nal of Geophysical Research: Space Physics*, *110*(A9). Retrieved from [http://](http://dx.doi.org/10.1029/2004JA010882)
534 dx.doi.org/10.1029/2004JA010882 (A09202) doi: 10.1029/2004JA010882
- 535 Tsyganenko, N. (1989). A solution of the chapman-ferraro problem for an el-
536 lipsoidal magnetopause. *Planetary and Space Science*, *37*(9), 1037 - 1046.
537 Retrieved from [http://www.sciencedirect.com/science/article/pii/](http://www.sciencedirect.com/science/article/pii/0032063389900767)
538 [0032063389900767](http://www.sciencedirect.com/science/article/pii/0032063389900767) doi: [http://dx.doi.org/10.1016/0032-0633\(89\)90076-7](http://dx.doi.org/10.1016/0032-0633(89)90076-7)